

Stability analysis and attractor dynamics of three-dimensional dark solitons with localized dissipation

Christian Baals ^{1,2} Alexandre Gil Moreno ¹ Jian Jiang,¹ Jens Benary ¹ and Herwig Ott ¹

¹*Department of Physics and Research Center OPTIMAS, Technische Universität Kaiserslautern, 67663 Kaiserslautern, Germany*

²*Graduate School Materials Science in Mainz, Staudinger Weg 9, 55128 Mainz, Germany*



(Received 22 December 2020; accepted 18 March 2021; published 2 April 2021)

We study the stability and the attractor dynamics of an elongated Bose-Einstein condensate (BEC) with dark or gray kink solitons in the presence of localized dissipation. To this end, the three-dimensional Gross–Pitaevskii equation with an additional imaginary potential is solved numerically. We analyze the suppression of the snaking instability in dependence of the dissipation strength and extract the threshold value for the stabilization of the dark soliton for experimentally realistic parameters. Below the threshold value, we observe the decay into a solitonic vortex. Above the stabilization threshold, we observe the attractor dynamics towards the dark soliton when initially starting from a gray soliton. We find that for all initial conditions the dark soliton is the unique steady-state of the system—even when starting from the BEC ground state.

DOI: [10.1103/PhysRevA.103.043304](https://doi.org/10.1103/PhysRevA.103.043304)

I. INTRODUCTION

Dissipative processes such as losses or decoherence are usually considered as a nuisance in quantum systems because they tend to destroy the coherence and drive the system from quantum to classical behavior [1]. This can become relevant even in well-isolated quantum systems such as ultracold atomic gases, where dissipative processes are strongly suppressed, but never absent. In recent years, open-system control of quantum matter has emerged as a new field of research, which perceives dissipative processes as a resource for quantum engineering and state preparation [2–10]. Such an approach requires that the desired quantum state is the dark state or steady-state of the system’s time evolution in the presence of an engineered dissipative process. If the dark state or steady state is unique, the system will evolve towards it, independent of the initial condition. This results in an attractor dynamics towards the steady state.

Here, we perform a realistic numerical experiment to study the stabilization and attractor dynamics of a dark soliton in an elongated, three-dimensional atomic Bose-Einstein condensate. We focus on two central questions:

(1) Can the dissipation be engineered in such a way that the dark soliton is stabilized under the system’s time evolution?

(2) Does the dissipation induce attractor dynamics towards the steady-state, irrespective of the initial conditions?

We show in this paper that both questions can be answered positively for experimentally realistic parameters. Our study exemplifies the concept of open-system control on a specific scenario and explicitly analyzes the emerging attractor dynamics.

The quantum system under consideration is a harmonically trapped Bose-Einstein condensate (BEC) of atoms, which we describe in the mean-field limit by means of the

three-dimensional (3D) Gross–Pitaevskii equation (GPE). We focus on dark kink-solitons (DSs) [11–14], which are stationary solutions of the GPE but dynamically unstable for a large variety of trapping frequencies [15,16]. Previous work in cylindrical trapping geometries has shown that the DS can decay into several different structures depending on the chemical potential and the radial trapping frequency [17]. Adding a local loss process, which we describe by an imaginary potential in the GPE, we study the time evolution of the DS for different strengths of the imaginary potential. A similar situation has been studied for the two-dimensional (2D) GPE. Here it has been shown that adding a one-dimensional (1D) Gaussian-shaped conservative repulsive potential can lead to the suppression of the snaking instability [18]. In one dimension, both studies in a 1D GPE system [5] and in a Bose-Hubbard system [7] show the emergence of a stable DS under these conditions. In addition, studies with parity-time-symmetric (\mathcal{PT} -symmetric) dipoles in 1D GPE systems have shown that, for certain dissipation strengths, moving light-gray solitons can be pinned [19]. For a \mathcal{PT} -symmetric Gaussian-shaped potential it has been shown that the DS is only stable within a certain range of imaginary potential heights. For too high imaginary potentials the interplay of gain and loss drives the system back to the ground state [20].

The stabilization and formation of DS by dissipation is not only relevant in the field of ultracold atoms as studied here but also in nonlinear optics. Mode-locked lasers, i.e., lasers with a fixed phase relation among the modes of the laser resonator, can be operated in a regime where they emit dark or gray pulses on top of a cw background. For correctly tuned parameters such as gain, loss, saturation energy and saturation power it can be shown within the power energy saturation model that the laser should emit dark pulses [21]. Experimentally, this has been observed for example with fiber lasers [22] or quantum dot lasers [23].

In this work, we map out the stability region for the DS, classify the emergent instability modes and characterize the attractor dynamics towards the DS. This work is inspired by previous experiments in our group [4,24], which serve as a guideline for the chosen parameters. Regarding the numerics, we efficiently solve the GPE on a GPU.

II. SYSTEM: THREE-DIMENSIONAL GROSS-PITAEVSKII EQUATION WITH IMAGINARY POTENTIAL

We consider a BEC subject to local losses within a mean-field theory, where the condensate order parameter is described by the Gross-Pitaevskii equation with imaginary potential (IGPE):

$$i\hbar \frac{\partial \Psi}{\partial t} = \left(-\frac{\hbar^2}{2m} \nabla^2 + V(\vec{r}) + g|\Psi|^2 - \frac{i\hbar}{2} \gamma(\vec{r}) \right) \Psi, \quad (1)$$

where $g = \frac{4\pi\hbar^2 a}{m}$ is the interaction strength, a is the s -wave scattering length,

$$V(\vec{r}) = \frac{1}{2}m(\omega_x^2 x^2 + \omega_y^2 y^2 + \omega_z^2 z^2) \quad (2)$$

is the 3D harmonic trapping potential, and $\gamma(\vec{r})$ describes the local particle losses. The number of particles N is given by the normalization condition $N = \int d\vec{r} |\Psi|^2$.

Such a scenario can be studied experimentally with a BEC and an additional scanning electron microscope [4,24] where a tightly focused electron beam removes and ionizes atoms from the BEC, which are subsequently extracted by an electric field and detected. This technique allows for a high-resolution manipulation of the BEC with—apart from the losses—almost negligible back-action on the BEC for a relatively long time. Previous studies [4,6] have shown that the IGPE [Eq. (1)] is indeed an adequate model to describe the system. To perform the numerical analysis with experimentally realistic parameters, we set the number of particles to $N = 80 \times 10^3$ and the trap frequencies to $(\omega_x, \omega_y, \omega_z) = 2\pi \times (12 \text{ Hz}, 170 \text{ Hz}, 170 \text{ Hz})$. We refer to the x coordinate as the axial direction and to y and z as the radial directions. We model the imaginary potential

$$\gamma(\vec{r}) = \gamma_0 \exp\left(-\frac{(x-x_0)^2}{2w_{\text{diss}}^2}\right) \quad (3)$$

as a Gaussian profile along the x axis (width w_{diss}) and as constant along the y and the z axis. Experimentally, this can be realized by scanning the electron beam (propagation direction z) along the y direction much faster than any intrinsic timescale of the BEC.

We solve the IGPE [Eq. (1)] numerically. To this end, we implement a time-splitting spectral method [25] in the programming language Julia. We use the package CUDA.jl [26,27] to run our simulations on a GPU (NVIDIA GeForce RTX 2060 Super) which results in a speed-up by a factor of about 20 compared with our CPU (HP Z620, 2x Intel XEON E5-2670).

III. STABILITY OF STATIONARY KINK SOLITONS

Dark kink solitons are stationary and dynamically stable solutions to Eq. (1) with $\gamma(\vec{r}) \equiv 0$ in 1D systems. When the

system becomes 3D, i.e., when the mean-field interparticle interaction exceeds the radial oscillation frequency by a critical value, they are still stationary solutions but become dynamically unstable. The so-called snaking instability then leads to a bending of the nodal plane of the soliton and eventually to its decay [15]. The stationary DS solutions can be written as $\Psi(\vec{r}, t) = e^{-\frac{i}{\hbar}\mu t} \psi(\vec{r})$ with the chemical potential μ . To find such a solution $\psi(\vec{r})$ we follow the idea given in Refs. [17,28] and start with an ansatz

$$\psi(\vec{r}) = \chi_{\text{TF}}(\vec{r}) \tanh\left(\frac{x}{\xi(\vec{r})}\right) \quad (4)$$

in the Thomas-Fermi regime where $\chi_{\text{TF}} = \sqrt{\mu_{\text{loc}}/g}$ is the Thomas-Fermi wave function with the local chemical potential $\mu_{\text{loc}} = \mu - V(\vec{r})$ and the local healing length $\xi(\vec{r}) = \hbar/\sqrt{m\mu_{\text{loc}}}$. Starting from Eq. (4) we find the DS solution to Eq. (1) numerically by employing imaginary time evolution.

Having found the stationary DS, we first consider the time evolution without localized dissipation. This has been studied already in Refs. [17,28] for a cylindrical trap. For the elongated harmonic trap that we study here, we expect qualitatively similar results since the potential in the axial direction does not change on the length scale of the soliton. Depending on the ratio of the chemical potential to the vibrational energy of the radial harmonic oscillator, the DS is either dynamically stable or unstable [17]. In our case we have $\mu = \hbar \times 6600 \text{ Hz}$ and thus a ratio $\frac{\mu}{\hbar\omega_{\perp}} = 6.2$. According to Refs. [17,28] we expect the DS to be dynamically unstable with two energetically lower lying states: a dynamically unstable single vortex ring (VR) and a dynamically stable solitonic vortex (SV). Indeed, this is what we observe when evolving the DS in time. Iso-surface plots of the density at characteristic points in time are shown in Fig. 1.

As a next step, we switch on the dissipation. We here restrict ourselves to experimentally accessible values and choose $w_{\text{diss}} = 130 \text{ nm}$ and $\gamma_0 \in [0, 7100] \text{ Hz}$ [4]. The amount of particles removed from the system during the time evolution is given by the overlap between the region of losses with the atomic density:

$$\dot{N} = - \int \gamma(\vec{r}) |\psi(\vec{r})|^2 d\vec{r}. \quad (5)$$

We can then identify the different stationary states (DS, VR, and SV) from the loss rate of particles because each of them has a characteristic density overlap with the loss region. In Fig. 2 we show the number of particles $N(t)$ in the condensate and the loss rate $\dot{N}(t)$ up to $t = 100 \text{ ms}$ for different dissipation strength γ_0 . Looking at $N(t)$ we see phases of linear decrease, connected by kinks. This behavior becomes more obvious for $\dot{N}(t)$, where this translates into plateaus. Up to $\gamma_0 = 2.4 \text{ kHz}$ two plateaus in \dot{N} (or two kinks in N) are visible. The first plateau with the lowest loss rate corresponds to the DS which has the lowest density overlap with the imaginary potential. The second plateau corresponds to the VR, which shows a higher loss rate. The highest loss rate is observed for the SV towards the end of the simulation time. Between $\gamma_0 = 2.4 \text{ kHz}$ and $\gamma_0 = 5.2 \text{ kHz}$ we observe only the decay into a VR within our computational time of 100 ms. For $\gamma_0 > 5.2 \text{ kHz}$ no decay is visible, which indicates the onset of

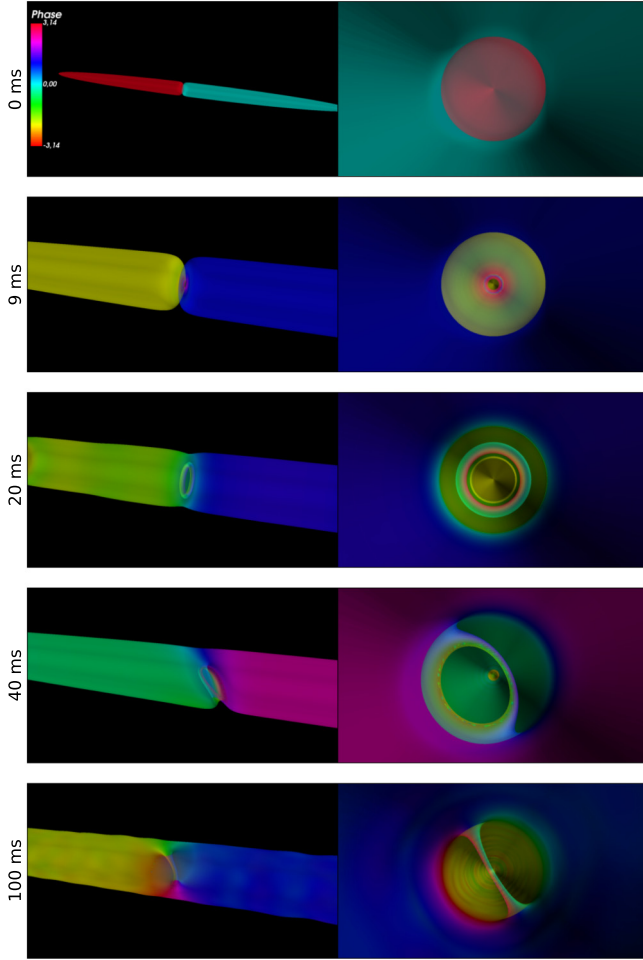


FIG. 1. Iso-surface plots of the DS without dissipation after different times. We show the density at 10% of its maximum as contours and the phase as color code. (top) Initial DS at $t = 0$ ms. After 9 ms the central plane of the DS starts to bend. This is the beginning of the snaking instability. After 20 ms the VR appears as an intermediate stationary state. Being unstable itself (see the bending and shift after 40 ms), it eventually decays into a solitonic vortex (100 ms), which is dynamically stable.

stabilization of the DS. This can also be seen in the behavior of $N(t)$ [see Fig. 2(c)], where the remaining number of atoms after $t = 100$ ms first decreases and then increases again for increasing dissipation strength. The decrease of $N(100$ ms) for $\gamma_0 > 5$ kHz is due to the finite width of the loss potential. The wings of the Gaussian overlap with regions of the BEC outside of the soliton such that a stronger loss potential leads to higher losses even with a DS. This is also visible in the final loss rate Fig. 2(d).

To quantify the decay process of the DS and to determine the threshold value of γ_0 for its stabilization, we analyze the minimum density in the center of the respective steady state. To this end, we integrate the density along the z direction, $|\tilde{\psi}(x, y)|^2 = \int |\psi(x, y, z)|^2 dz$ and numerically determine the axial position of the density minimum, $x_{\min} = \min(|\tilde{\psi}(x, 0)|^2)$. The result is shown in Fig. 3(a). We observe that the DS remains at its position at the center of the BEC, whereas the VR and the SV move away from the center. To

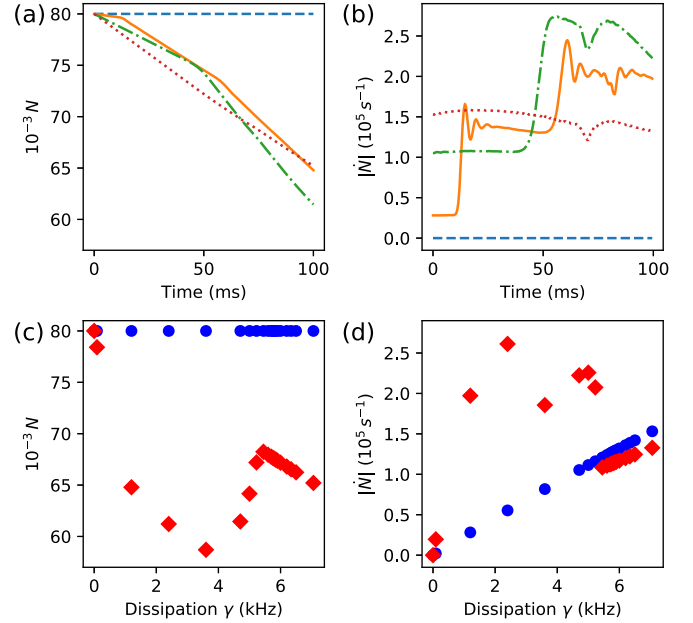


FIG. 2. (a) Number of particles N and (b) loss rate $|\dot{N}|$ over time for characteristic dissipation strengths $\gamma_0 = 0$ kHz (blue dashed line), $\gamma_0 = 1.2$ kHz (orange solid line), $\gamma_0 = 4.7$ kHz (green dash-dotted line) and $\gamma_0 = 7.1$ kHz (red dotted line). The local maximum of \dot{N} at 83 ms is due to a density wave that is created due to the finite extent of the dissipative potential [6]. It travels towards the edge of the BEC gets reflected there and returns towards the imaginary potential. (c) Number of particles N and (d) loss rate $|\dot{N}|$ at $t = 0$ ms (blue points) and at $t = 100$ ms (red diamonds).

further quantify the dynamics of the decay of the DS, we consider the integrated density of the slice at x_{\min} , i.e., $n = \int |\psi(x_{\min}, y, z)|^2 dy dz$ and compare it to the integrated density of such a slice at the axial center of the ground-state wave function, i.e., $n_0 = \int |\psi_{\text{gs}}(0, y, z)|^2 dy dz$. The relative density at the position of the soliton is then defined by $n_{\text{rel}} = \frac{n}{n_0}$. This is shown in Fig. 3(b). Again, we can identify the three different solitary waves: the DS with the lowest density, the VR with an intermediate density and the SV with the highest density. To extract the decay time τ of the DS we fit the initial dynamics of $n_{\text{rel}}(t)$ with an exponential function $A \exp(-\frac{t}{\tau})$. We restrict the time to t_{max} where $n_{\text{rel}}(t_{\text{max}}) = 1\%$. The result of the fit is shown as a solid line in Fig. 3(d). One can clearly see that the initial dynamics shows an exponential behavior. Note the large dynamic range over which the density is changing. The initial decrease of n_{rel} for high γ_0 where the DS is stabilized in Fig. 3(d) originates from the fact that the DS and the imaginary potential do not yet perfectly overlap. Thus, there is an initial reduction of the density until the system has reached its steady state.

The fitted decay time τ is shown in Fig. 4 over γ_0 . We see that τ increases with increasing γ_0 up to a critical point γ_{crit} before it drops. This is typical for a critical slowing down, described by an algebraic behavior of the form

$$\tau = a \left(\frac{|\gamma - \gamma_{\text{crit}}|}{\gamma_{\text{crit}}} \right)^b. \quad (6)$$

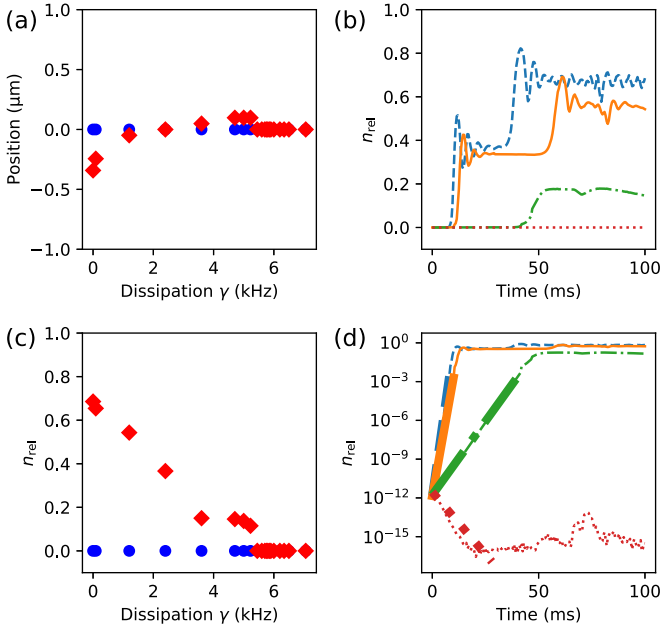


FIG. 3. Analysis of the decay of the DS. (a) Position of the density minimum at $t = 0$ ms (blue points) and $t = 100$ ms (red diamonds) for different γ . For large γ , the dark soliton is stable and the density minimum does not move. For small γ , the final structure (VR or SV) has moved away from the center. (b) Time evolution of the radially integrated density in the density minimum for characteristic dissipation strengths $\gamma_0 = 0$ kHz (blue dashed line), $\gamma_0 = 1.2$ kHz (orange solid line), $\gamma_0 = 4.7$ kHz (green dash-dotted line), and $\gamma_0 = 7.1$ kHz (red dotted line). The three solitary waves have distinct values of the density. (c) Radially integrated relative density in the density minimum after $t = 0$ ms (blue points) and $t = 100$ ms (red diamonds) for different γ . As in panel (a) the initial and final values overlap above γ_{crit} . (d) Exponential fit of the initial part of the dynamics from panel (b) to extract the decay time of the DS.

Fitting this model to our data, we find $\gamma_{\text{crit}} = 5893$ Hz, $a = 3.60 \times 10^{-4}$ s, and a critical exponent of $b = -1.12$. The data and the fit are shown in Fig. 4(b).

So far we have only considered one set of parameters for N and $(\omega_x, \omega_y, \omega_z)$ in our simulations. In a realistic experiment, however, fluctuations of the particle number N occur and the harmonic trap might not be radially isotropic. To get an idea of how γ_{crit} depends on these parameters we conduct two additional sets of simulations. In the first one we set $N = 40 \times 10^3$ and keep the radially isotropic trap frequencies at $(\omega_x, \omega_y, \omega_z) = 2\pi \times (12 \text{ Hz}, 170 \text{ Hz}, 170 \text{ Hz})$. In the second one we keep $N = 80 \times 10^3$ and set a radially anisotropic trap with frequencies $(\omega_x, \omega_y, \omega_z) = 2\pi \times (12 \text{ Hz}, 160 \text{ Hz}, 180 \text{ Hz})$. These frequencies are realistic values for the experiment of Refs. [4,24] if we add the influence of gravity on the optical dipole trap. In both cases we also observe the stabilization of the DS as shown in Fig. 4. For the anisotropic trap with $N = 80 \times 10^3$ we find $\gamma_{\text{crit}} = 5909$ Hz, $a = 3.84 \times 10^{-4}$ s, and $b = -0.95$. Here it is interesting to point out that without dissipation and for low γ the DS first decays into a deformed VR, then into two parallel vortices which eventually merge to a single stable SV. For the isotropic

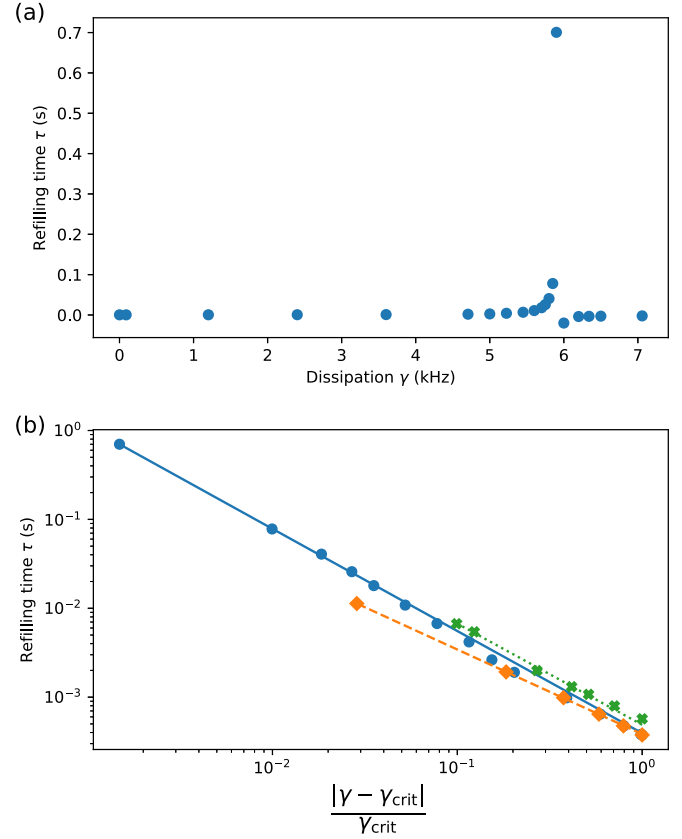


FIG. 4. (a) Refilling time extracted from an exponential fit to the initial dynamics of n_{rel} over dissipation γ [compare Fig. 3(d)] for $N = 80 \times 10^3$ particles in a radially isotropic trap. (b) Same data (blue points) rescaled by $\gamma_{\text{crit}} = 5893$ Hz and plotted logarithmically together with a power-law fit (blue solid line). Additional simulations with $N = 80 \times 10^3$ particles in a radially anisotropic trap (orange diamonds and dashed line, $\gamma_{\text{crit}} = 5909$ Hz) and $N = 40 \times 10^3$ particles in a radially isotropic trap (green crosses and dotted line, $\gamma_{\text{crit}} = 4107$ Hz).

trap with $N = 40 \times 10^3$ we find $\gamma_{\text{crit}} = 4107$ Hz, $a = 4.88 \times 10^{-4}$ s, and $b = -1.14$. Since we have here a ratio $\frac{\mu}{\hbar\omega_{\perp}} = 4.7$ we observe the same structures (i.e., VR and SV) to which the DS decays for $\gamma(\vec{r}) \equiv 0$, in agreement with Ref. [28].

IV. ATTRACTOR DYNAMICS TOWARDS THE DARK KINK SOLITONS

Having established that the dark soliton is the steady state of the system for $\gamma > \gamma_{\text{crit}}$, we now analyze its attractor dynamics. To this end, we consider two different dissipation strengths: $\gamma_{0,<} = 1200$ Hz which is below the stabilization threshold for the DS and $\gamma_{0,>} = 7100$ Hz which is above the stabilization threshold. As initial conditions, we chose different gray kink solitons (GKSs) and study their time evolution under the influence of dissipation. To construct proper initial states, we start from the wave function of the ground state ψ_{gs} in the harmonic trap. To obtain a wave function which is close to the GKS we multiply the ground-state wave function by the function which describes a moving DS in a homogenous

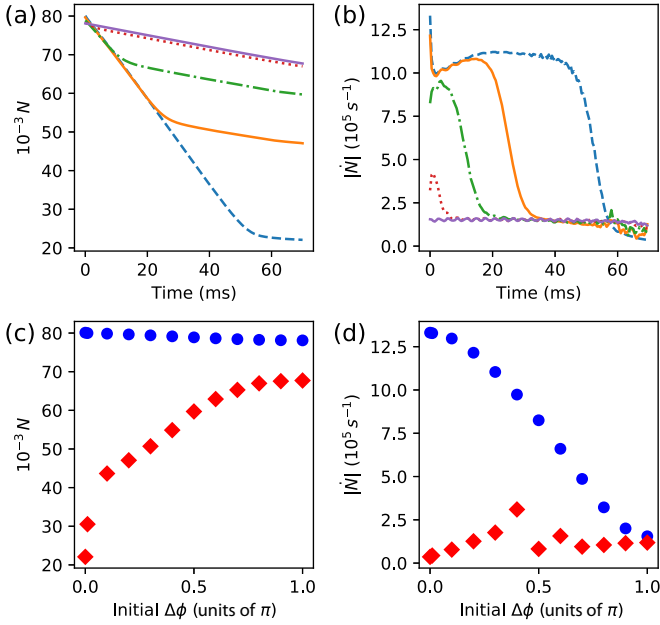


FIG. 5. Attractor dynamics towards the dark soliton. (a) Number of particles $N(t)$ and (b) loss rate $|\dot{N}(t)|$ for different initial phase difference $\Delta\phi$ of the gray kink soliton, i.e., $\Delta\phi = 0$ (blue dashed line), $\Delta\phi = 0.2\pi$ [orange lower solid line in panel (a) and orange upper solid line in panel (b)], $\Delta\phi = 0.5\pi$ (green dash-dotted line), $\Delta\phi = 0.8\pi$ (red dotted line), and $\Delta\phi = \pi$ [violet upper solid line in panel (a) and violet lower solid line in panel (b)]. (c) Number of particles $N(t)$ and (d) loss rate $|\dot{N}(t)|$ at $t = 0$ ms (blue points) and $t = 70$ ms (red diamonds).

background, i.e.,

$$\psi_{\text{GKS}}(x, y, z) = \psi_{\text{gs}}(x, y, z) \times \left[\tilde{v} - i\sqrt{1 - \tilde{v}^2} \tanh\left(\frac{x}{\xi(x, y, z)}\sqrt{1 - \tilde{v}^2}\right) \right], \quad (7)$$

where \tilde{v} is the velocity of the GKS in units of the speed of sound. This is related to the phase difference far away from the kink by

$$\Delta\phi = \phi(x \rightarrow \infty) - \phi(x \rightarrow -\infty) = -2 \arccos(\tilde{v}). \quad (8)$$

The local healing length is denoted by $\xi(x, y, z)$. In the following, we choose the full range of possible phase differences between the two ends of the wave function, $\Delta\phi \in [0, \pi]$. This way, we can sample all initial states interpolating between the BEC ground state and the DS. To be sensitive to instability modes, we add for the evolution of the ground state 5% of Gaussian noise before evolving in time.

For $\gamma_{0,<}$ we see qualitatively the same behavior as described in Ref. [17]: The GKS oscillates in the trap and eventually decays. No attractor dynamics is visible. The situation changes for $\gamma_{0,>}$. In Fig. 5 the number of particles $N(t)$ and the loss rate $\dot{N}(t)$ over time are shown for the different initial phase differences $\Delta\phi$. The evolution of the atom number shows that the initial losses are reduced, if the GKS gets closer to the DS, which features the lowest amount of losses. We can also see that the total atom number shows a kink, after

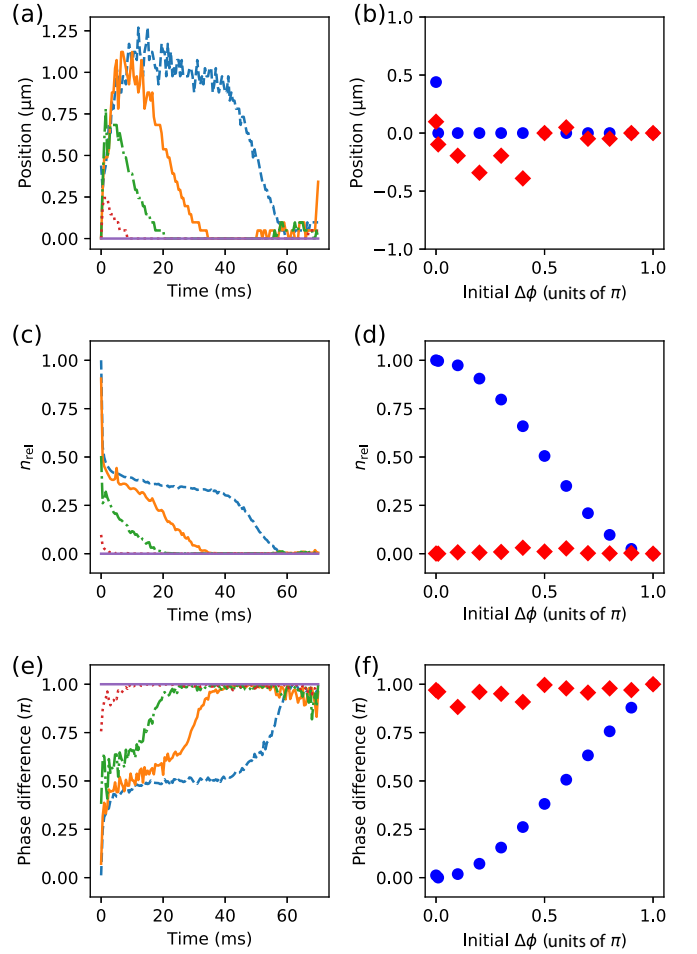


FIG. 6. Attractor dynamics towards the dark soliton. (a) Evolution of the position of the density minimum at different initial phase differences $\Delta\phi = 0$ (blue dashed line), $\Delta\phi = 0.2\pi$ (orange upper solid line), $\Delta\phi = 0.5\pi$ (green dash-dotted line), $\Delta\phi = 0.8\pi$ (red dotted line), and $\Delta\phi = \pi$ (violet lower solid line). The initial motion of the gray soliton is damped and the DS is stabilized at the central position, where the dissipation is located for all initial phase differences as shown in (b) for the position at $t = 0$ ms (blue points) and $t = 70$ ms (red diamonds). (c) The density in the minimum approaches zero [color code as that of panel (a)] over time and for all initial phase differences (d) [color code is the same as that of panel (b)]. (e) The phase difference across the density minimum approaches the characteristic value of π of the DS [color code is the same as that of panel (a) but with the upper solid line for $\Delta\phi = \pi$ and the lower solid line for $\Delta\phi = 0.2\pi$] over time and for all initial phase differences (f) [color code is the same as that of panel (b)].

which the losses are reduced. This shows the appearance of a stable DS, which becomes more visible if we look at the loss rate $|\dot{N}(t)|$ in Fig. 5(b). For all initial $\Delta\phi$ we observe the same $|\dot{N}|$ after 70 ms, signaling the attraction to the same steady state. This can be also seen in the initial and final number of atoms and loss rate in Fig. 5(c) and 5(d).

To further verify the attraction towards a DS we find the plane of minimal density in axial direction as described in Sec. III and plot its position [Figs. 6(a) and 6(b)] and its relative density [Figs. 6(c) and 6(d)]. We see that, for low phase differences, the GKS moves away from the center

and is attracted back towards the location of the dissipation at $x = 0$. Also, n_{rel} approaches the minimum value of the DS. Finally we consider the phase difference which we define as $\Delta\phi(t) = \arg(\psi(x_{\text{min}} + 1 \mu\text{m}, 0, 0)) - \arg(\psi(x_{\text{min}} - 1 \mu\text{m}, 0, 0))$. In Figs. 6(e) and 6(f) we see that this approaches π for all $\Delta\phi(t = 70 \text{ ms})$. That is, the wave function is attracted towards the DS. Our results show that the DS is the unique steady-state for a whole class of initial states and even the condensate ground state is attracted towards it.

V. DISCUSSION AND CONCLUSIONS

We studied the dynamics of a 3D Bose-Einstein condensate with a dark or a gray kink soliton in an elongated trap with localized dissipation. In the case of the dark soliton, we find that the snaking instability is suppressed above a certain threshold value of the dissipation strength. For the gray soliton, we observe an attraction of the system towards the dark soliton. We find that the dark soliton is the unique steady state for all initial gray solitons, even when starting from the BEC ground

state. Performing numerical experiments, we cannot, however, exclude, that another steady state exists for the given parameters. The existence of such a state would be intriguing, as one could observe and study bistable behavior in the system. To generalize our work, it would be interesting to perform a linear stability analysis on the two situations presented here within the framework of a Bogoliubov transformation and see how the imaginary frequencies become suppressed with increasing dissipation strength. This would help to establish the full phase diagram of the system and to relate our findings to dissipative phase transitions.

ACKNOWLEDGMENTS

We gratefully acknowledge discussions with Joachim Brand, Antonio Muñoz Mateo, Corinna Kollath and Ian Spielman. We acknowledge financial support by the Deutsche Forschungsgemeinschaft within the collaborative research center TRR 185, project B3 (number 277625399), and within the graduate school of excellence MAINZ.

-
- [1] H.-P. Breuer and F. Petruccione, *The Theory of Open Quantum Systems* (Oxford University Press, Oxford, 2007).
 - [2] S. Diehl, A. Micheli, A. Kantian, B. Kraus, H. P. Büchler, and P. Zoller, Quantum states and phases in driven open quantum systems with cold atoms, *Nat. Phys.* **4**, 878 (2008).
 - [3] S. Diehl, A. Tomadin, A. Micheli, R. Fazio, and P. Zoller, Dynamical Phase Transitions and Instabilities in Open Atomic Many-Body Systems, *Phys. Rev. Lett.* **105**, 015702 (2010).
 - [4] G. Barontini, R. Labouvie, F. Stubenrauch, A. Vogler, V. Guarrera, and H. Ott, Controlling the Dynamics of an Open Many-Body Quantum System with Localized Dissipation, *Phys. Rev. Lett.* **110**, 035302 (2013).
 - [5] V. A. Brazhnyi, V. V. Konotop, V. M. Pérez-García, and H. Ott, Dissipation-Induced Coherent Structures in Bose-Einstein Condensates, *Phys. Rev. Lett.* **102**, 144101 (2009).
 - [6] A. Müllers, B. Santra, C. Baals, J. Jiang, J. Benary, R. Labouvie, D. A. Zezyulin, V. V. Konotop, and H. Ott, Coherent perfect absorption of nonlinear matter waves, *Sci. Adv.* **4**, eaat6539 (2018).
 - [7] F. Trimborn, D. Witthaut, H. Hennig, G. Kordas, T. Geisel, and S. Wimberger, Decay of a Bose-Einstein condensate in a dissipative lattice—the mean-field approximation and beyond, *Eur. Phys. J. D* **63**, 63 (2011).
 - [8] D. Witthaut, F. Trimborn, H. Hennig, G. Kordas, T. Geisel, and S. Wimberger, Beyond mean-field dynamics in open Bose-Hubbard chains, *Phys. Rev. A* **83**, 063608 (2011).
 - [9] P. Barmettler and C. Kollath, Controllable manipulation and detection of local densities and bipartite entanglement in a quantum gas by a dissipative defect, *Phys. Rev. A* **84**, 041606(R) (2011).
 - [10] H. Fröml, A. Chiochetta, C. Kollath, and S. Diehl, Fluctuation-Induced Quantum Zeno Effect, *Phys. Rev. Lett.* **122**, 040402 (2019).
 - [11] S. Burger, K. Bongs, S. Dettmer, W. Ertmer, K. Sengstock, A. Sanpera, G. V. Shlyapnikov, and M. Lewenstein, Dark Solitons in Bose-Einstein Condensates, *Phys. Rev. Lett.* **83**, 5198 (1999).
 - [12] C. Becker, S. Stellmer, P. Soltan-Panahi, S. Dörscher, M. Baumert, E.-M. Richter, J. Kronjäger, K. Bongs, and K. Sengstock, Oscillations and interactions of dark and dark-bright solitons in Bose-Einstein condensates, *Nat. Phys.* **4**, 496 (2008).
 - [13] A. R. Fritsch, M. Lu, G. H. Reid, A. M. Piñeiro, and I. B. Spielman, Creating solitons with controllable and near-zero velocity in Bose-Einstein condensates, *Phys. Rev. A* **101**, 053629 (2020).
 - [14] D. J. Frantzeskakis, Dark solitons in atomic Bose-Einstein condensates: From theory to experiments, *J. Phys. A: Math. Theor.* **43**, 213001 (2010).
 - [15] A. E. Muryshev, H. B. van Linden van den Heuvell, and G. V. Shlyapnikov, Stability of standing matter waves in a trap, *Phys. Rev. A* **60**, R2665(R) (1999).
 - [16] J. Brand and W. P. Reinhardt, Solitonic vortices and the fundamental modes of the “snake instability”: Possibility of observation in the gaseous Bose-Einstein condensate, *Phys. Rev. A* **65**, 043612 (2002).
 - [17] A. M. Mateo and J. Brand, Stability and dispersion relations of three-dimensional solitary waves in trapped Bose-Einstein condensates, *New J. Phys.* **17**, 125013 (2015).
 - [18] M. Ma, R. Carretero-González, P. G. Kevrekidis, D. J. Frantzeskakis, and B. A. Malomed, Controlling the transverse instability of dark solitons and nucleation of vortices by a potential barrier, *Phys. Rev. A* **82**, 023621 (2010).
 - [19] N. Karjanto, W. Hanif, B. A. Malomed, and H. Susanto, Interactions of bright and dark solitons with localized \mathcal{PT} -symmetric potentials, *Chaos* **25**, 023112 (2015).
 - [20] V. Achilleos, P. G. Kevrekidis, D. J. Frantzeskakis, and R. Carretero-González, Dark solitons and vortices in \mathcal{PT} -symmetric nonlinear media: From spontaneous symmetry breaking to nonlinear \mathcal{PT} phase transitions, *Phys. Rev. A* **86**, 013808 (2012).
 - [21] M. J. Ablowitz, S. D. Nixon, T. P. Horikis, and D. J. Frantzeskakis, Dark solitons of the power-energy saturation

- model: Application to mode-locked lasers, *J. Phys. A: Math. Theor.* **46**, 095201 (2013).
- [22] H. Zhang, D. Y. Tang, L. M. Zhao, and X. Wu, Dark pulse emission of a fiber laser, *Phys. Rev. A* **80**, 045803 (2009).
- [23] M. Feng, K. L. Silverman, R. P. Mirin, and S. T. Cundiff, Dark pulse quantum dot diode laser, *Opt. Express* **18**, 13385 (2010).
- [24] T. Gericke, P. Würtz, D. Reitz, C. Utfeld, and H. Ott, All-optical formation of a Bose-Einstein condensate for applications in scanning electron microscopy, *Appl. Phys. B: Lasers Opt.* **89**, 447 (2007).
- [25] W. Bao, S. Jin, and P. A. Markowich, On time-splitting spectral approximations for the Schrödinger equation in the semiclassical regime, *J. Comput. Phys.* **175**, 487 (2002).
- [26] T. Besard, C. Foket, and B. De Sutter, Effective extensible programming: Unleashing Julia on GPUs, *IEEE Trans. Parallel Distrib. Syst.* **30**, 827 (2018).
- [27] T. Besard, V. Churavy, A. Edelman, and B. De Sutter, Rapid software prototyping for heterogeneous and distributed platforms, *Adv. Eng. Softw.* **132**, 29 (2019).
- [28] A. Muñoz Mateo and J. Brand, Chladni Solitons and the Onset of the Snaking Instability for Dark Solitons in Confined Superfluids, *Phys. Rev. Lett.* **113**, 255302 (2014).